



ARL-TR-7344 • JULY 2015



Enhanced Thermal Transport of Surfaces with Superhydrophobic Coatings

by Thomas C Parker, Joshua R Mitchell, and Joseph P Labukas

Approved for public release; distribution is unlimited.

NOTICES

Disclaimers

The findings in this report are not to be construed as an official Department of the Army position unless so designated by other authorized documents.

Citation of manufacturer's or trade names does not constitute an official endorsement or approval of the use thereof.

Destroy this report when it is no longer needed. Do not return it to the originator.



Enhanced Thermal Transport of Surfaces with Superhydrophobic Coatings

by Thomas C Parker and Joseph P Labukas
Weapons and Materials Research Directorate, ARL

Joshua R Mitchell
Oak Ridge Institute for Science and Education, Belcamp, MD

REPORT DOCUMENTATION PAGE

Form Approved
OMB No. 0704-0188

Public reporting burden for this collection of information is estimated to average 1 hour per response, including the time for reviewing instructions, searching existing data sources, gathering and maintaining the data needed, and completing and reviewing the collection information. Send comments regarding this burden estimate or any other aspect of this collection of information, including suggestions for reducing the burden, to Department of Defense, Washington Headquarters Services, Directorate for Information Operations and Reports (0704-0188), 1215 Jefferson Davis Highway, Suite 1204, Arlington, VA 22202-4302. Respondents should be aware that notwithstanding any other provision of law, no person shall be subject to any penalty for failing to comply with a collection of information if it does not display a currently valid OMB control number.

PLEASE DO NOT RETURN YOUR FORM TO THE ABOVE ADDRESS.

1. REPORT DATE (DD-MM-YYYY) July 2015		2. REPORT TYPE Final		3. DATES COVERED (From - To) September 2014	
4. TITLE AND SUBTITLE Enhanced Thermal Transport of Surfaces with Superhydrophobic Coatings				5a. CONTRACT NUMBER	
				5b. GRANT NUMBER	
				5c. PROGRAM ELEMENT NUMBER	
6. AUTHOR(S) Thomas C Parker, Joshua R Mitchell, and Joseph P Labukas				5d. PROJECT NUMBER	
				5e. TASK NUMBER	
				5f. WORK UNIT NUMBER	
7. PERFORMING ORGANIZATION NAME(S) AND ADDRESS(ES) US Army Research Laboratory ATTN: RDRL-WMM-C Aberdeen Proving Ground, MD 21005-5069				8. PERFORMING ORGANIZATION REPORT NUMBER ARL-TR-7344	
9. SPONSORING/MONITORING AGENCY NAME(S) AND ADDRESS(ES)				10. SPONSOR/MONITOR'S ACRONYM(S)	
				11. SPONSOR/MONITOR'S REPORT NUMBER(S)	
12. DISTRIBUTION/AVAILABILITY STATEMENT Approved for public release; distribution is unlimited.					
13. SUPPLEMENTARY NOTES					
14. ABSTRACT Hydrophobic and superhydrophobic coatings/surfaces are often found in natural systems. These surfaces provide functional advantages, such as self-cleaning and water collection. In this work we show enhanced thermal transport of a copper tube with a superhydrophobic coating. We attribute this enhanced thermal transport to a reduced water layer thickness on the superhydrophobic surface. We used an idealized thermal transport model and showed that the predicted thermal transport rate agreed quantitatively with the observed transport rate and water layer thickness.					
15. SUBJECT TERMS thermal transport, superhydrophobic, jumping droplet, cooling, nanostructure, self-assembled monolayer					
16. SECURITY CLASSIFICATION OF:			17. LIMITATION OF ABSTRACT	18. NUMBER OF PAGES	19a. NAME OF RESPONSIBLE PERSON
a. REPORT	b. ABSTRACT	c. THIS PAGE			Thomas C Parker
Unclassified	Unclassified	Unclassified	UU	16	19b. TELEPHONE NUMBER (Include area code) 410-306-0870

Contents

List of Figures	iv
1. Introduction	1
2. Technical Approach	2
2.1 Electrodeposition	2
2.2 Copper Cleaning Silver Deposition	4
2.3 SAM Deposition	4
3. Results/Analysis	5
4. Conclusion	7
5. References	8
Distribution List	9

List of Figures

Fig. 1	Contact angle	1
Fig. 2	Enhanced heat transfer from superhydrophobic coating	5
Fig. 3	Power dissipated vs. water layer thickness	7

1. Introduction

In the literature, one of the most cited examples of a natural superhydrophobic surface is the lotus leaf (*Nelumbo nucifera*). The static contact angle of water droplets placed on the surface of the lotus leaf is 160° .¹ Superhydrophobic surfaces have potential applications in self-cleaning surfaces,² corrosion-resistant materials, low-friction surfaces,³ and for use as thermal diodes.⁴

Artificial hydrophobic surfaces are inspired by naturally occurring water-repellent surfaces, such as the lotus leaf and the wings of a cicada.^{1,5,6} In cases when the energy of the surface on which a water droplet is resting is lower than the surface energy inside the droplet, the surface will tend toward hydrophobicity. It has been found that creating a low-energy surface on a 2-phase substrate with 2-phase roughness (nano and micrometer scale) will tend to create a superhydrophobic surface.²

The characterization of hydrophobicity is done by measuring the contact angle of a drop of water on the surface. The wettability of a surface can be assessed by measuring the contact angle (σ) formed between a droplet of liquid and the surface (Fig. 1). Qualitatively, surfaces with a water contact angle less than 90° can be considered hydrophilic, and surfaces with a water contact angle greater than 90° are hydrophobic.² In reviewing the literature, there seems to be a consensus: a surface is superhydrophobic if the contact angle exceeds 150° .^{2,6}

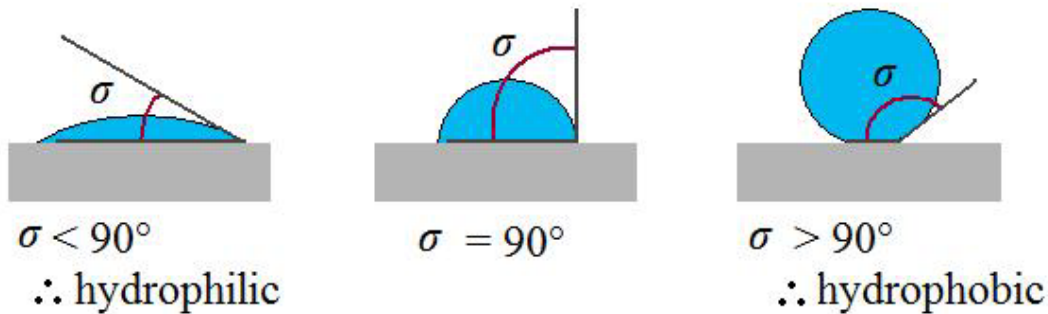


Fig. 1 Contact angle

The contact angle can be modeled using Young's equation shown as Eq. 1. Minimization of Gibb's free energy can be related to the balance of the interfacial interaction energies, which is given in Eq. 1. The interfacial energy between the solid surface (gray in Fig. 1) and the gas (air) is γ_{SG} , the interfacial energy between the solid and liquid is γ_{SL} , and the interfacial energy between the liquid and the gas is γ_{LG} . Typically in an experiment, γ_{LG} and γ_{SG} are static and γ_{SL} is modified through changes in the surface morphology and/or surface chemistry. The angle (σ) is then measured as depicted in Fig. 1 and used to measure the solid-liquid interface energy.

$$\gamma_{SG} - \gamma_{SL} - \gamma_{LG} \cos \sigma = 0 . \quad (1)$$

2. Technical Approach

In this research we use the method described by Larmour⁷ to prepare superhydrophobic surfaces. This is a relatively simple process that consists of 3 steps. The first step is the substrate preparation, where the copper (Cu) surface is clean of contaminants and its oxide layer. Next, silver (Ag) is deposited using electrodeless electrochemical deposition to form a rough surface with a fractal-like geometry. Finally, the surface chemistry is modified from a hydrophilic chemistry (oxide) to a hydrophobic surface using a fluorinated (or protonated) self-assembled monolayer (SAM). Chemical attachment to the Ag surface is accomplished with a thiol end group.⁷⁻⁹

The goals of this work were to provide a deeper insight into the 3 steps in this process. More specifically, the types of substrates that can be used to synthesize superhydrophobic surfaces (i.e., electrodeposited, evaporated, and bulk metal) and the deposition conditions for the silver and SAM layer were investigated. The high rates of water removal from superhydrophobic surfaces via the jumping droplet mechanism and contact angle were investigated as a method to increase heat removal from a Cu tube.

2.1 Electrodeposition

The substrates used for our electrochemical deposition were 2-inch-diameter 304-2B stainless steel discs supplied by Q-Lab Corporation. The as-received discs were polished using 1,200-grit silicon carbide sandpaper, rinsed for several seconds with ethanol, then rinsed for several seconds with deionized (DI) water, and finally dried with compressed filtered nitrogen. Prior to the electrochemical deposition, the sample was selectively masked. The back side of the sample was masked off with Kapton tape to avoid plating on this “back” surface and a horizontal strip across the middle of the front of the disk. The front piece allowed for a distinct cutoff between the plated half and unplated half of the disc, giving an overall surface area of 10.13 cm² to be plated. The resultant step edge from the deposited Cu to the stainless steel substrate was later used (postdeposition) to measure the deposited Cu film thickness with atomic force microscopy and stylus profilometry.

The plating solution used was obtained by combining 200 mL of 0.01-M Cu II sulfate, 50 mL of 1-M sodium sulfate, and 50 mL of 0.1-M sulfuric acid in a 500-mL beaker. According to the Pourbaix diagram for Cu, an acidic solution can help ensure that the various oxides of Cu are avoided during the deposition process so that only a uniform layer of the 2+ oxidation state of Cu is deposited on to the substrate. At 25 °C only a mildly acidic solution is required (pH < 5.5); as such, the solution used was able to be kept between a pH of 2 and 3, well below the required

limit. The electroplating process of Cu in this environment is diffusion limited, a small (3.5 cm) polyethylene-coated magnetic stir bar was left running during the entire process at roughly 300–500 rpm to maintain a low-compliance voltage between 0.7 and 1 V. Significantly higher compliance voltages can cause secondary electrochemical reactions to occur, such as the electrolysis of water and the evolution of hydrogen.

To decrease the contact resistance between the disc and the cathode wire of the potentiostat, a 1-cm² piece of Cu foil was used. The foil was polished with 600 then 1,200 grit sandpaper and rinsed for several seconds with acetone followed by ethanol then DI water. The foil was then folded around the top of the unmasked portion of the disc.

The cathode wire was attached, via clean alligator clip, to the Cu foil on the stainless steel disc; the anode wire was similarly attached to a clean high-quality Cu bar (dimensions 8 × 2 × 0.5 cm). We then mounted both the anode and the cathode, using electrical tape, into a custom sample holder made of high-density polyethylene. This sample holder was designed to fit the 500-mL beaker, ensuring the sample and Cu anode were secure and that the front surfaces were parallel. Using a 3-pronged lab clamp, we next lowered the sample holder into the agitating plating solution so that the disc was half submerged in plating solution and neither of the alligator clamps was in contact with the solution.

The calculation of deposition rates of Cu was solved using Eq. 1, which was derived from Faraday’s laws of electrolysis:

$$R = \frac{I \times M}{F \times z \times D \times A} \times 1 \times 10^7 \frac{nm}{cm}, \quad (2)$$

where

R = deposition rate (nm/s)

I = current (mA)

M = molar mass of Cu (63.54 g/mol)

F = Faraday’s constant, (96485 C/mol)

z = oxidation number (Cu II = 2)

D = density (Cu at room temperature 8.96 g/cm³)

A = area on which to be deposited (cm²)

To ensure the growth of a uniform Cu layer on the stainless steel substrate, the cell was initially run for 11 min in galvanostatic stepper mode with a cycled current of

0.5 mA for 16 ms then 0 mA for 4 ms. Using Eq. 1, we find that the expected yield of Cu thickness is 10 nm.

Immediately following the stepped deposition, the potentiostat was switched to direct galvanostatic mode and run at 20-mA current, giving a current density of $1.97 \text{ mA}\cdot\text{cm}^{-2}$, for 22 min and 45 s, for a calculated Cu thickness of 990 nm.

The Cu-plated substrate was removed from the holder, rinsed with DI water for 10 s, then dried with compressed filtered nitrogen. The Kapton tape was then carefully removed.

2.2 Copper Cleaning Silver Deposition

To produce the first tier of the requisite 2-tiered roughness for superhydrophobicity, the Cu surfaces described previously were immersed in a 0.1-M aqueous solution of hydrochloric acid for 1 min. The samples were then rinsed with DI water for several seconds and dried with filtered nitrogen. The samples were then immersed in 0.01-M aqueous solution of silver nitrate for 20 s. The deposition occurs because of the displacement of Cu to the silver ions, $\text{Cu} + 2\text{AgNO}_3 \rightarrow \text{Cu}(\text{NO}_3)_2 + 2\text{Ag}$. The reaction is diffusion-limited, so the solution was agitated, via swirling, to allow for an even coverage of silver over the treated surface of the substrate. It was found early on that if agitation was not employed an uneven webbing pattern of silver formed on the surface of the substrate. The samples were then rinsed with DI water for several seconds and dried with filtered nitrogen.

2.3 SAM Deposition

The final step involved the deposition of a self-assembled monolayer onto the silvered surface of the substrate. In following with previous procedures carried out at Duke University, solutions were made using dichloromethane; however, several tests showed that ethanol could be a suitable solvent. The silvered samples were immersed in 0.001-M 1H,1H,2H,2H-perfluorodecanethiol, in dichloromethane, for 10 min, rinsed with dichloromethane, then ethanol, then DI water, and then dried with nitrogen.

Water contact angles were measured to be less than 170° .

In a separate experiment, a polished Cu pipe was treated with hydrochloric acid, silver nitrate, and fluorinated SAM as above.

3. Results/Analysis

The top image in Fig. 2 shows the 0.25-inch-diameter Cu tube coated with the superhydrophobic surface. The bottom image shows an untreated 0.25-inch-diameter Cu tube. Cold water enters the inner diameter of the tubes from the left and exits to the right. As the water transits the tube, it absorbs heat from the surrounding warm/moist air (30 °C at ~100% relative humidity). At a flow rate of 4 gal/h (or ~4.2 g of H₂O/s), the temperature increases through the superhydrophobic coating (SHC) tube and untreated tube are 1° ± 0.1 °C and 0.5° ± 0.1 °C, respectively. Using the heat capacity of water 4.18 J/g-centigrade, we can readily calculate the total power heating the water to be 17.8 ± 1.8 W for the SHC-treated tube and 8.8 ± 1.8 W for the untreated tube. It is hypothesized that the difference in the heat transfer rate is due to the insulating properties of the condensed water layer on the outer diameter of the tube.

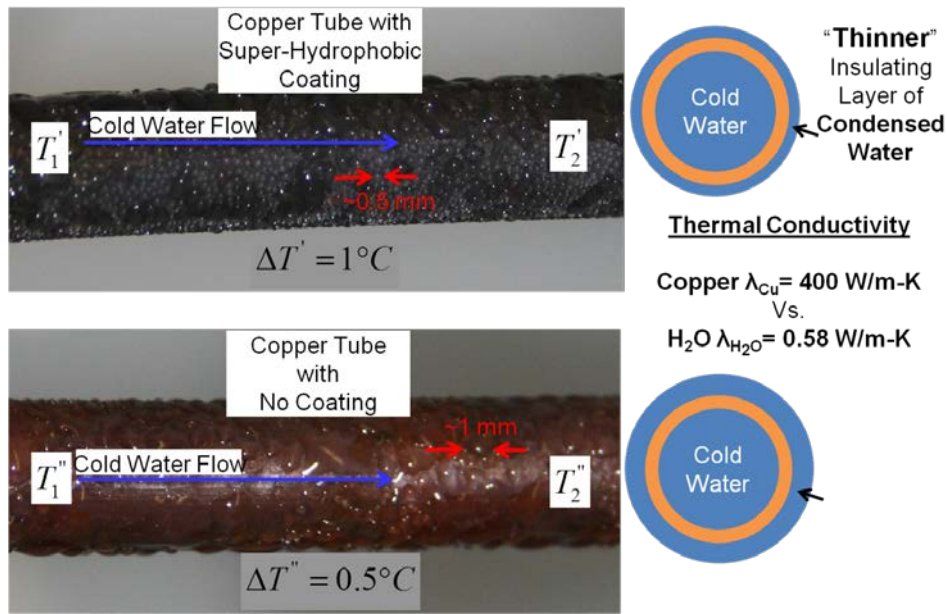


Fig. 2 Enhanced heat transfer from superhydrophobic coating

From the images it can be seen that, on average, the SHC tube has smaller-diameter water droplets than the untreated tube, where the size of the condensate on the SHC is on the order of 0.5 mm versus approximately 1 mm on the untreated tube. The exact water layer thickness is difficult to ascertain, but it is clear from the optical images that the 0.5- to 1-mm sizes are in the correct size regimes.

Using Eq. 2, we can calculate the total power (heat) transferred across a material (Cu in this case): 16,208 W. We have assumed that both the heat source and the heat sink are modeled as having infinite thermal conductivity. The total power in

watts is equal to the cross-sectional surface area (0.00253 m^2) of the exposed outer surface of the cold Cu tube with the surrounding hot air multiplied by the thermal conductivity of Cu ($\lambda_{Cu} = 400 \text{ W/m}\cdot\text{K}$) and the temperature difference ($\Delta T = 20 \text{ K}$) between the cold water within the Cu tube and the surrounding air divided by the thickness of the Cu ($t_{Cu} = 0.813 \text{ mm}$).

$$Power(\text{watts}) = \frac{S.A.\lambda_{Cu}\Delta T}{t_{cu}} . \quad (3)$$

Equation 4 gives the total power (heat) transferred across a Cu tube with a water layer (condensation) on the outer surface of the Cu tube. In our setup, the cross-sectional SA again is equal to 0.00253 m^2 , the thermal conductivity of H_2O (λ_{H_2O}) is $0.58 \text{ W/m}\cdot\text{K}$, the thermal conductivity of Cu (λ_{Cu}) is $400 \text{ W/m}\cdot\text{K}$, the temperature difference ΔT is 20 K , and the Cu tube wall thickness (t_{Cu}) is fixed at 0.813 mm .

$$Power(\text{watts}) = \frac{S.A.\Delta T}{\frac{t_{Cu}}{\lambda_{Cu}} + \frac{t_{H_2O}}{\lambda_{H_2O}}} . \quad (4)$$

The blue solid curve in Fig. 3 is a plot of Eq. 4 versus water layer thickness (t_{H_2O}). The red line (dot-dash) shows the thermal conductivity for a Cu tube as determined using Eq. 3. The horizontal line at 17.6 W shows the measured thermal dissipation for the SHC sample, and the horizontal line at 8.8 W shows the measured thermal dissipation for the uncoated sample. From this plot it is clear that the overall thermal dissipation is strongly dependent on the water layer thickness. If we correlate our measured thermal dissipation (17.6 and 8.8 W) with the theoretical water layer thickness, we get approximately 1.1 and 2 mm , respectively. Our approximate water layer thickness estimated from the images in Fig. 3 qualitatively agrees very well. The quantitative differences can be explained by some of our model assumptions, such as the source and sink having infinite thermal conductivity.

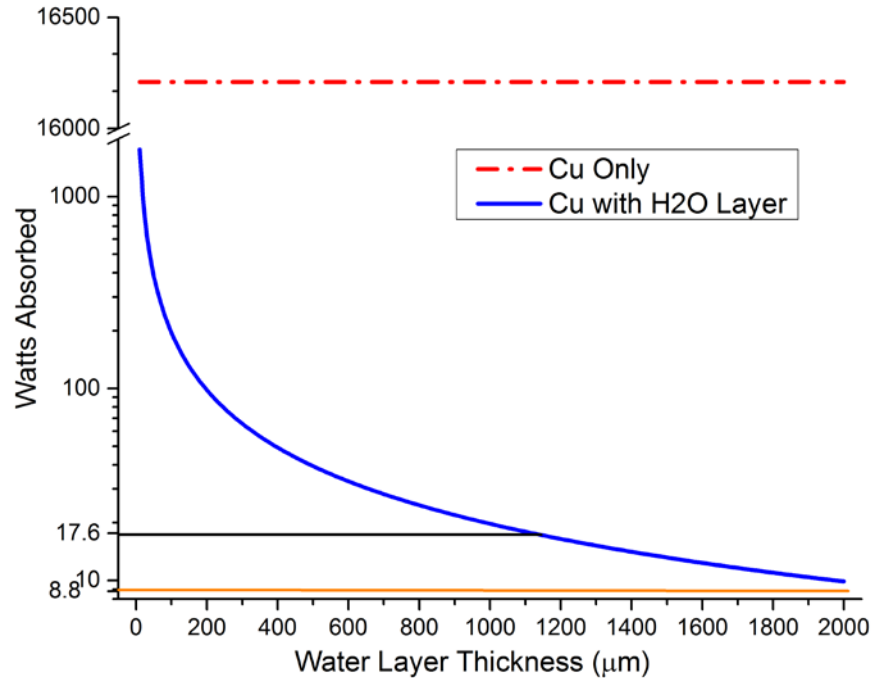


Fig. 3 Power dissipated vs. water layer thickness

4. Conclusion

We have shown the ability to coat nonplanar substrates (Cu tubes) with an SHC. The condensed water droplets on these SHC-treated tubes exhibited jumping droplet behavior. We observed a significant difference in the water droplet radius of the condensed water on SHC versus uncoated tubes. The SHC-coated tubes exhibited significantly high thermal transport rates. The enhanced thermal transport was attributed to a thinner water layer on the surface of the SHC tubes. The measurement thermal transport was modelling using a relatively simple model consisting of 2 conduction materials in series (Cu and water). The model agreed quantitatively with the observed water layer thickness and the measured thermal transport, indicating the very strong dependence of the water layer thickness on the overall thermal transport.

5. References

1. Marmur A. The lotus effect: superhydrophobicity and metastability. *Langmuir*. 2004;20(9):3517–3519. doi: 10.1021/la036369u.
2. Crick CR, Parkin IP. Preparation and characterisation of super-hydrophobic surfaces. *Chemistry - A European Journal*. 2010;16(12):3568–3588. doi: 10.1002/chem.200903335.
3. Weng C-J, Peng C-W, Chang C-H, Chang Y-H, Yeh J-M. Corrosion resistance conferred by superhydrophobic fluorinated polyacrylate-silica composite coatings on cold-rolled steel. *Journal of Applied Polymer Science*. 2012;126(S2). doi: 10.1002/app.36380.
4. Boreyko JB, Chen C-H. Self-propelled jumping drops on superhydrophobic surfaces. *Physics of Fluids*. 2010;22(9). doi: 10.1063/1.3483222.
5. Sun M, Watson GS, Zheng Y, Watson JA, Liang A. Wetting properties on nanostructured surfaces of cicada wings. *Journal of Experimental Biology*. 2009;212(19):3148–3155. doi: 10.1242/jeb.033373.
6. Forch R, Schonherr H, Jenkins ATA, editors. *Surface design: applications in bioscience and nanotechnology*. Weinheim (Germany): Wiley-VCH Verlag GmbH & Co. KGaA; 2009. doi: 10.1002/9783527628599.
7. Larmour IA, Bell SEJ, Saunders GC. Remarkably simple fabrication of superhydrophobic surfaces using electroless galvanic deposition. *Angewandte Chemie International Edition*. 2007;46(10):1710–1712. doi: 10.1002/anie.200604596.
8. Love CJ, Estroff LA, Kriebel JK, Nuzzo RG, Whitesides GM. Self-assembled monolayers of thiolates on metals as a form of nanotechnology. *ChemInform*. 2005;36. doi: 10.1002/chin.200532281.
9. Chen C-H, Cai Q, Tsai C, Chen C-L, Xiong G, Yu Y, Ren Z. Dropwise condensation on superhydrophobic surfaces with two-tier roughness. *Applied Physics Letters*. 2007;90(17). doi: 10.1063/1.2731434.

1 DEFENSE TECHNICAL
(PDF) INFORMATION CTR
DTIC OCA

2 DIRECTOR
(PDF) US ARMY RESEARCH LAB
RDRL CIO LL
IMAL HRA MAIL & RECORDS
MGMT

1 GOVT PRINTG OFC
(PDF) A MALHOTRA

13 DIR USARL
(PDF) RDRL WMM
R DOWDING
J ZABINSKI
RDRL WMM B
D KNORR
J SANDS
E WETZEL
RDRL WMM C
J DEMAREE
J LABUKAS
J LA SCALA
J MITCHELL
T PARKER
RDRL WMM G
J ORLICKI
A RAWLETT
J SNYDER

INTENTIONALLY LEFT BLANK